International Journal of Technology 15(4) 1162-1172 (2024)
Received March 2022 / Revised March 2022 / Accepted April 2022

International Journal of Technology

http://ijtech.eng.ui.ac.id

Residual Stress and Texture Analysis of Leaf Spring Failure

Andoko Andoko[1 *], Pradhana Kurniawan[2], Suprayitno Suprayitno[1], Femiana Gapsari[3], Maykel Manawan[4]

[1]*Department of Mechanical and Industrial Engineering, State University of Malang, Jl. Semarang No. 5, 65146 Malang, Indonesia*
[2]*Department of Mechanical Engineering, Faculty of Engineering, University of Merdeka Malang, Jl. Terusan Raya Dieng 62-64, 65146, Indonesia*
[3]*Department of Mechanical Engineering, Brawijaya University, Jl. Veteran No. 16, 65146, Malang, Indonesia*
[4]*Physics Department, Science Faculty, Pertahanan University, IPSC Sentul Sukahati, 16810, Bogor, Indonesia*

Abstract. The leaf spring fabrication process, which consists of various processes, will result in susceptibility to atomic defects. Therefore, the identification of defects at the atomic scale through crystallography is very important in analyzing the slip mechanism to minimize the occurrence of leaf spring failure. This study aimed to analyze the causes of leaf spring failure by crystallography through an experimental approach. Residual stress testing was carried out using XRD with the sin 2φ approach. The Sin 2φ method uses angles -20°, -16°, -12°, -4°, 0°, 4°, 12°, 16°, 20°. Crystal orientation and texture were performed using MAUD 2.94 software to analyze the Miller index and crystallographic orientation distribution. Hardness test using Vickers micro with indentation points near and far from the leaf spring fracture surface. Leaf spring fracture morphology was tested using a DSLR camera and Scanning Electron Microscopy (SEM). The results of the residual stress analysis show a wavy elliptical curve indicating that the broken leaf spring has a shear stress and a stress gradient. The resulting residual stress has compressive properties with a value of -278.5±17.4 with the resulting crystal orientation consisting of miller index planes (110), (200), (211). The crystal orientation plane (200) has a characteristic texture that is oriented towards the Normal Direction (ND). Normal direction is indicated by a high probability value of 1.20. A high probability indicates that the leaf spring has material surface defects. The void is the beginning of the formation of crack initiation and becomes the center of stress concentration.

Keywords: Failure; Leaf spring; Residual stress; Texture

1. Introduction

Leaf springs are mostly used in heavy vehicle suspension systems because of their low cost, easy maintenance, ability to accept higher loads and good vibration damping (Kurniawan *et al.,* 2021; Kong *et al.,* 2016; Scuracchio, de-Lima, and Schön, 2013). The vibrations generated from the road surface and wheels are suppressed by the leaf springs so that they are not transmitted to the vehicle body and are stored in elastic deformation (Andoko, Puspitasari, and Permanasari, 2017). These conditions make the leaf spring material must have the characteristics of a combination of high strength and fatigue resistance.

*Corresponding author's email: andoko.ft@um.ac.id, Tel.: +62812-3352726
doi: 10.14716/ijtech.v15i4.5571

The process of making leaf springs consists of several processes, namely the selection of raw materials, mechanical formation, heat treatment and surface treatment (Scuracchio Scuracchio, de-Lima, and Schön, 2013). The fabrication process that is not well controlled will cause non-uniform plastic deformation (residual stress) and microscopic defects (Božić, Schmauder, and Wolf, 2018; De-la-Rosa *et al.,* 2016). The presence of residual stress and microscopic defects with the breaking of bond chains can affect the deterioration of the behavioral characteristics of the material.

Residual stress consists of two types, namely compressive residual stress and tensile residual stress (Soyama, Chighizola, and Hill, 2021; Fairfax and Steinzig, 2016). Compressive residual stress is beneficial for leaf springs because, together with strain hardening, it can increase fatigue life resistance (Xiao *et al.,* 2022; Soyama *et al.,* 2011). Residual tensile stress is detrimental because it impacts the formation of crack initiation and the faster crack growth rate (Božić, Schmauder, and Wolf, 2018). The residual compressive stress generated in the shot peening process will have an impact on increasing the fatigue resistance of leaf springs (Shojaei *et al.,* 2021). Increased fatigue resistance is carried out through a shot peening process with different depths of decaburization (Chadwick, 2016). The low carburizing depth indicates an elastic deformation mechanism, whereas, at a higher decaburization depth, there will be plastic deformation which contributes to the compressive residual stress. Surface depths up to 0.02 mm of compressive residual stress directly affect fatigue crack nucleation (Scuracchio, de-Lima, and Schön, 2013). Fabrication behavior such as cold press can increase tensile residual stress and dislocation. High residual stress at the location of stress concentration will accelerate the occurrence of failure (Pástor *et al.,* 2020).

Various studies on residual stress have attracted the attention of researchers in increasing the fatigue strength of leaf springs. Besides fatigue strength, other characteristics such as strength, stress corrosion cracking and deformation are also highly dependent on the pole figure texture of the material (Wenk, 2016). Pole figure texture is a graphical representation of the orientation of objects in space by recording the intensity of the given Bragg reflection as a function of the rotation and slope of the sample (Ren *et al.,* 2021; Bunge, 2013). The results of the graphic image through the X-Ray Diffraction experimental method will produce a preferred crystal orientation that can affect the material properties. Material properties that have low strength occur when the material's texture pattern is imperfect, which will create weaknesses in the crystal lattice structure and cause failure (Liu *et al.,* 2018). The development of microstructure, mechanical properties and texture on automotive grade AISI 4130 steel is through the austenitization process (Heidary *et al.,* 2020). Texture components change substantially by changing the austempering temperature and time. Hot-rolled steel has higher strength but lower ductility in TD (transverse direction) (Li *et al.,* 2021). The effect of crystallographic texture is seen in the anisotropic properties of hot-rolled steel (Chen *et al.,* 2020). Anisotropy with a lower Taylor factor value in austenite along the RD (rolling direction) will result in the formation of an early slip.

This study intends to provide novelty findings related to residual stress analysis and crystallography for further failure analysis on leaf springs. This study aimed to analyze the cause of the failure of a broken leaf spring through an experimental method. Experimental methods include residual stress analysis, crystal orientation, texture, hardness and fracture morphology. The experimental analysis results are useful in further improving the leaf springs' mechanical properties.

2. Methods

2.1. Materials

The fracture of the leaf spring material used in this study (Figure 1) from a Mitsubishi L300 vehicle (PT. Indospring Tbk, East Java, Indonesia).

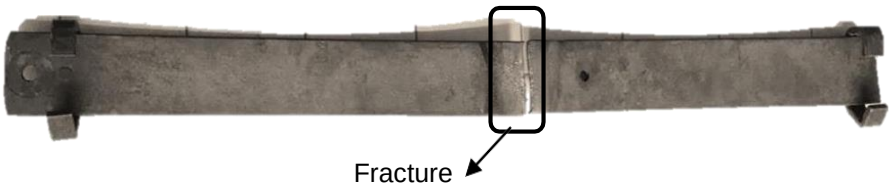

Figure 1 Leaf Spring Failed

2.2. Chemical Composition

The chemical composition of the broken leaf springs was analyzed using a spectrometer (Hilger Emissions, Type E-9 OA701, Margate, UK). The specimens were standardized with ASTM E 350 testing. The chemical composition of the leaf material can be seen in Table 1, which will then be compared with the standardization of spring steel material.

Table 1 Chemical Composition of Leaf Spring Material

Material	C (%)	Si (%)	Mn (%)	P (%)	S (%)	Cr (%)	V (%)
leaf spring	0.492	0.164	0.754	0.024	0.0100	0.661	0.15 – 0.25

The results of the chemical composition test (Table 1) show that the failed leaf spring materials are grade spring steel with SUP 10 standardization (C = 0,47 – 0,55%, Si = 0,15 – 0,35% Mn = 0,65 – 0,95%, P= ≤0,035%, S = ≤0,035%, Cr = 0,80 -1,10% and V = 0,15 – 0,250%).

2.3. Residual Stress, Crystal Orientation and Texture

Residual stress testing was performed using XRD (Bruker, Type D8 Advance, Karlsruhe, Germany). The residual stress test was measured using the sin2ψ method with angles (ψ) -20°, -16°, -12°, -4°, 0°, 4°, 12°, 16°, 20° (Figure 2 a). The test was carried out with Cu-Kα1 radiation, wavelength 1.5046 and the test was carried out with the standardization of ASTM E2860. the remaining size connection in the crystal orientation plane (211), a 5 second step speed in an angle of 2θ = 99.69. The XRD data was then processed using Qualx 2.1 and MAUD 2.94 software to analyze the smoothness, crystal orientation and texture. The texture is plotted into two parts, namely the polar image texture and the inverted polar image based on ND (Normal Direction), TD (Transverse Direction) and RD (Rolling Direction).

2.4. Hardness Test

Hardness testing was done with several leaf spring material indentation points using the Micro Vickers Hardness Tester Machine (Mitutoyo, Type HM-200, Kanagawa, Japan). The indentation points start near the fracture and away from the fracture in Figure 2b. This test used the micro Vickers method with ASTM E 384 standardization.

2.5. Fracture Morphology

Morphological observations, both macroscopically and microscopically, were carried out to analyze the characteristics of the fracture form—macro photo using a camera (Canon DSLR, Type EOS 1300D, Tokyo, Japan). Fracture morphology using Scanning (SEM) (Field Electron and Ion Company Hillsboro, Type Inspect-S50, Oregon, United States) with ASTM STP 827 standardization.

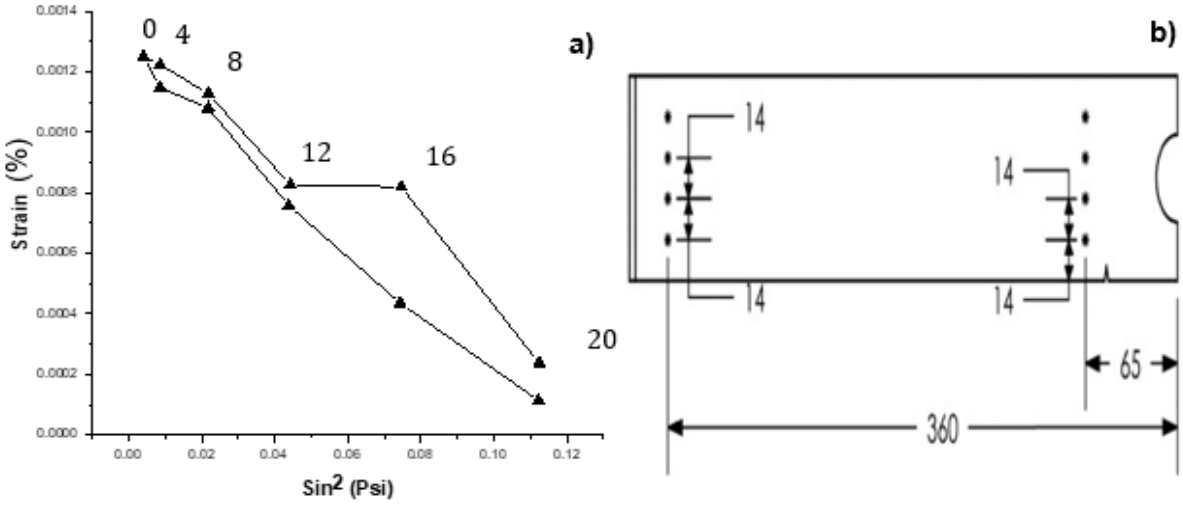

Figure 2 a) Residual Stress Test Results b) Position of Hardness Indentation Point

3. Results

3.1. Residual Stress

The results of the XRD Residual Stress diffraction image on the broken leaf spring can be seen in Figure 3a. The highest intensity was produced at an angle ψ of -20° and the lowest at an angle of 20°. The XRD data results were then used for FWHM analysis (Table 2). Table 2 shows that with increasing negative angle (psi), the intensity/peak produced is higher. Increasing the angle reduces the intensity, so the FWHM (full-width half maximum) parameter is needed to identify the effect.

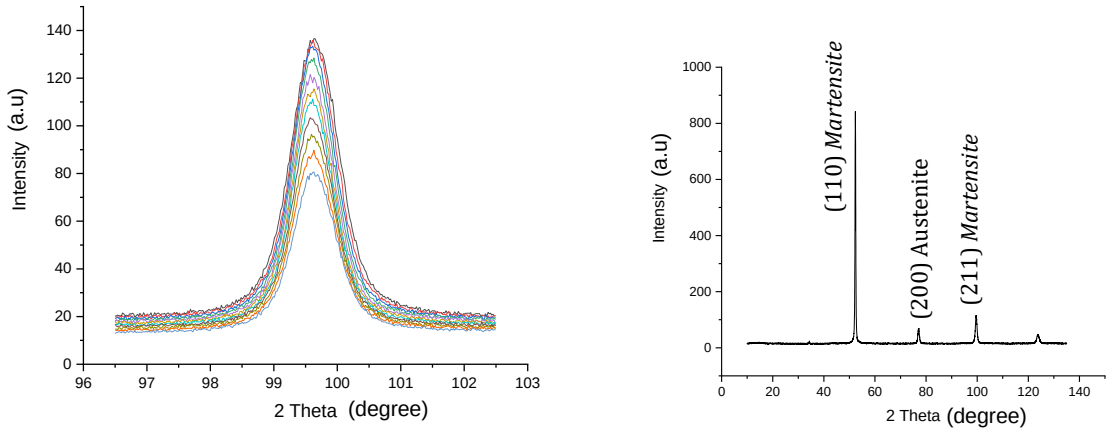

Figure 3 a) Peak Diffraction Results from Residual Stress b) XRD results of a broken leaf spring

The residual stress measurement data is then plotted on a graph of strain versus 2ψ, as shown in Figure 2a. Figure 2a shows an elliptical category curve with normal stress on a negative slope. The shear stress (blue curve) is elliptical, and the texture shows a wavy curve. Elliptical curves are defined as splitting as evidence of the presence of shear stress. Shear stress is generated due to the mechanical surface treatment of leaf springs, such as rolling. The resulting shear stress on the curve above is 5±1.7, while the normal stress generated is -278.5±17.4.

Table 2 Results of FWHM Residual Stress

K	λ	2θ (˚)	ψ (˚)	FWHM β (˚)
		99.65	-20	0.93
		99.64	-16	0.88
		99.63	-12	0.85
		99.63	-8	0.83
		99.62	-4	0.82
0.94	1.51	99.62	0	0.81
		99.62	4	0.82
		99.63	8	0.82
		99.63	12	0.83
		99.63	16	0.84
		99.65	20	0.85

3.2. Crystal Orientation

Based on the results of the sequential research field refinement (Figure 3b), the largest peak angle is produced at an angle of 2θ = 52.36˚ with a crystal orientation of (110). Crystal plane (211) with angle 2θ = 99.65˚ and crystal plane (200) with angle 2θ=77.19˚ Crystal orientation (110) resulted in high crystal size and spacing (Table 3). High lattice strains and dislocations were produced at the crystal orientation (200). Crystal orientation (211) has the lowest dislocation and lattice strain.

Table 3 Results of Crystal Orientation, Microstrain and Dislocation

Crystal Orientation					*Crystallite Size* (nm)	*Lattice Strain*	Dislocation
h	k	l	2θ	FWHM β (˚)			
1	1	0	52.34	0.37	28.9	0.0033	0.0012
2	0	0	77.09	0.73	16.8	0.0039	0.0036
2	1	1	99.62	0.83	17.9	0.0031	0.0032

3.3. Texture

Figure 4 shows the figure texture plot of the failed leaf spring surface. Based on the analysis of the characteristics of the pole figure, the crystal orientation of (200) has the highest probability compared to (110) and (211).

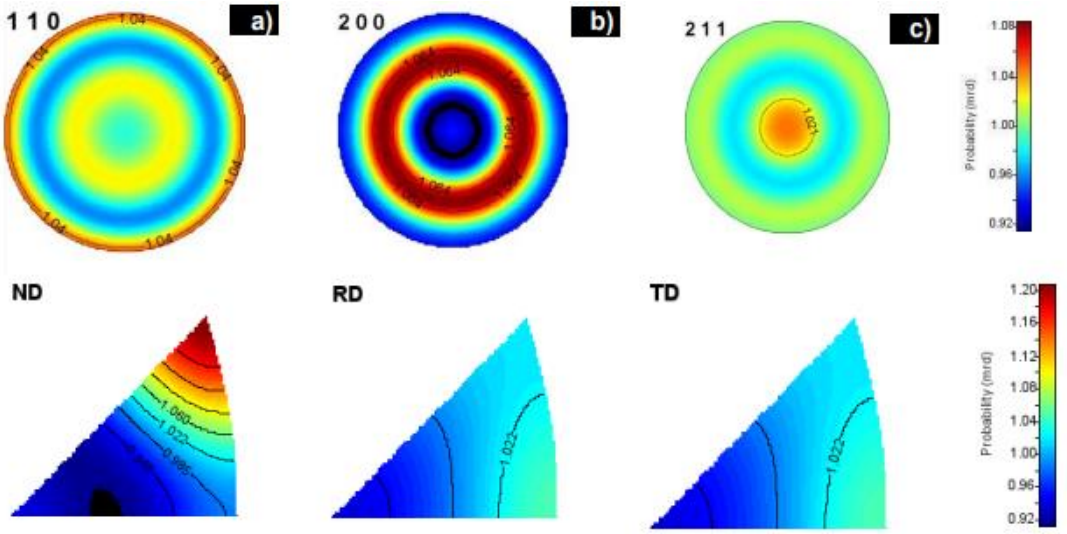

Figure 4 a) Crystal Oriented Texture (110) and Inverse on ND (110) b) Crystal Oriented Texture (200) and Inverse on RD (200) c) Crystal Oriented Texture (211) and Inverse on ND (211)

3.4. Hardness

The results of the hardness of the failed leaf spring can be seen in Table 4. Based on the results of the hardness test on the leaf spring shows that the hardness near the fracture has a higher value than that at the distance of the fracture.

Table 4 Leaf Spring Material Hardness Test Results

	Hardness Vickers Number (HV)				Average
	1	2	3	4	
Near Fracture	478	485	473	489	481.25
Away Fracture	427	400	425	407	414.75

4. Discussion

Previous studies on the analysis of the causes of leaf spring failure have only been investigated through general experimental characteristics of materials, such as analysis of the chemical composition, microstructure, hardness and fracture morphology. However, this study will analyze the failure further through residual stress, crystal orientation and texture. This condition was investigated because the leaf spring has a complex manufacturing process. This process will likely occur atomic defects and residual tensile stresses, which reduce fatigue strength. Based on testing the chemical composition of the leaf spring material, it is included in the standard specification for spring steel SUP 10. The composition of C, Si, Mn, P and S is in the range of SUP 10 spring steel materials. However, the Cr element is slightly below the SUP 10 standard, and V has a high amount. The low Cr element will impact the slow transformation of austenite to ferrite (Zhang *et al.,* 2019). Ferrite and residual austenite are ductile constituents which are more ductile than martensite (Xie *et al.,* 2020). The amount of ferrite and residual austenite, which is dominant compared to martensite, will have an adverse effect on reducing fatigue strength (Fuentes *et al.,* 2009). These conditions indicate that the quenching process in the leaf spring is imperfect due to various factors such as temperature austenitization time and cooling rate (Peng *et al.,* 2010). Martensite is also affected by the high alloy content after the cold rolling process and impacts increasing the degree of strain-induced martensite (SIM) (Anwar *et al.,* 2021). This imperfection can also be seen from the hardness results near and far from the fracture, which has a difference of 22.1%, where the position near the fracture has a higher value than the standard spring steel JASO C 601 (406 – 448). Uncontrolled local heating of the leaf springs during the rolling, bending and heat treatment processes causes decaburization and softening at some points on the surface. The high hardness of the part near the fracture causes the material characteristics to become more brittle and reduces the ductility of the leaf spring. The decrease in ductility impacts the decrease in the elasticity function of the leaf spring at the time of maximum loading so that it can cause crack initiation (Fragoudakis *et al.,* 2013). Higher hardness is synonymous with increased tensile strength, where the microstructure grains under these conditions are finer (Abdul *et al.,* 2021; Purnama *et al.,* 2020).

The high hardness of the leaf spring surface is identical to the martensite microstructure. The more dominant martensite microstructure is also seen in crystal orientation and texture results. The crystal orientation with the highest peak resulted in the (110) plane, which is identical to the martensite tetragonality based on the correspondence between the crystal structures (fcc) and (bcc). (001) fcc // (001) bcc. (010) fcc // (-110)bcc (Chen *et al.,* 2020). The martensite phase consists of the (110) and (211) planes, while the austenite is in the (200) plane. According to research by Hossain et al., the peak of austenite occurs in the (200) plane, and when compressive residual stress occurs,

the peak of austenite decreases (Hossain *et al.,* 2016). This condition makes martensite increase in the (110) field. The increase in the distance 'd' corresponds to the increase in lattice parameters, which will come from thermal expansion during the leaf spring heating process (Ahn *et al.,* 2020). The lattice vector (110) is the shortest lattice plane owned by the bcc phase. Where the plane connects the atom at the cubic angle to the middle atom and is a certain slip direction (Ren *et al.,* 2021; Bunge, 2013). The (110) plane is the slip that frequently occurs (three fields of type (110) intersect in the (111) direction). Therefore, the screw dislocation can move in all three (110) planes, so the slip line is often wavy. The resulting texture in the (110) plane has a probability of less than 2. It can be concluded that the leaf spring material has isotropic characteristics (Manawan *et al.,* 2021). Isotropic refers to the property of a material having uniformity of direction. These properties are reinforced by the resulting residual stress. Residual stress shows compressive compared to shear stress. A more dominant compressive residual stress will prevent the shear stress from failing (Minamizawa *et al.,* 2022). The compressive residual stress will impact the material's mechanical properties, such as reducing the crack growth rate. The driving force in initiating growth becomes greater, and the crack growth effect decreases significantly with an increasing stress ratio (Fragoudakis, Savaidis, and Michailidis, 2017).

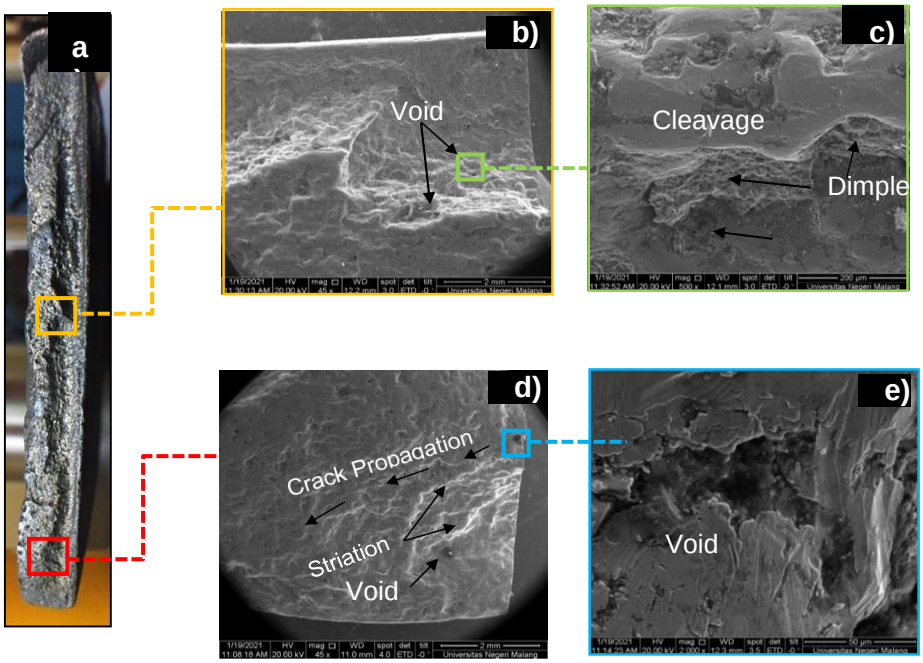

Figure 5 a) Macro photo of the surface of a broken leaf spring, b) The orange dashed line is a 45 x magnification at the center of the fault surface, c) The green dashed line is a 500 x magnification of the part of the fault surface indicated by the green box, d) The red dashed line is a 45 x magnification at the end of the fault surface, e) The blue dashed line is a 500 x magnification of the fault surface marked with a blue box

Crack initiation is done by observing the fracture morphology through macro and micro. The fracture morphology shows that crack initiation originates from voids evenly distributed on the leaf spring surface. Voids originating from material defects are most susceptible to dynamic loading and trigger the formation of crack nucleation and become the center of stress concentration. The initiation of voids causes brittleness of the martensite phase in the steel microstructure (Kadkhodapour, Butz, and Rad, 2011). The formation of voids often occurs in the fracture of martensite lath particles and interfacial decohesion (Zhang *et al.,* 2015). Intercritically treated structural fractures in medium carbon steels indicate that martensitic interfacial decohesion is the main mode of

nucleation and void growth (Bag, Lévesque, and Brochu, 2020). Three modes of formation of void nucleation, namely martensite crack, ferrite-martensite interface decohesion, and ferrite-ferrite interface decohesion with minimum plastic deformation (Xie *et al.,* 2020). The higher stress concentration in the voids due to fatigue loading will impact crack propagation. Fatigue crack propagation can be seen based on benchmarks and striations (Aliakbari, 2019). The striations indicate slow crack propagation due to compressive residual stress and good ductility. Good ductility was demonstrated on SEM observations by the presence of uneven surfaces and dimple fractures (Figure 5b and Figure 5d).

The resulting compressive residual stress is related to the slope of the elliptical curve on the strain versus the 2ψ graph. The slope of the ellipse to the left indicates that the microstrain is negative. The negative microstrain value is related to the distance between the crystal planes, which are identical on the atomic scale; there is no local distortion in the lattice plane (Bruno *et al.,* 2011). This condition shows that the microstrain that occurs is more dominantly uniform. Microstrain uniformity can also be seen in the (110) and (211) crystal planes. The (200) crystal planes have different microstrains and indicate possible defects. Indications of defects show a sudden change in the arrangement of atoms at low-stress levels, and an irregular crystallographic texture occurs (Li *et al.,* 2021). The crystallographic texture in the (200) plane also has a high probability, and means that the field has a weak texture. Weak texture (200) occurs due to the deformation of the rolling process (Priyanto, Effendi, and Parikin, 2015). The weak texture is related to the presence of voids (Figure 5b and 5c) in the fracture morphology. Voids will trigger stress concentrations, impact strength reduction and fatigue, and become the initial formation of crack nucleation (Andoko, 2019). The crack then propagates based on the movement of the direction of the striations, which can be seen in Figure 5d.

5. Conclusions

This study aimed to analyze the causes of leaf spring failure through residual stress, crystal orientation, texture, hardness and fracture morphology. Residual stress shows compressive properties with a value of -278.5 ± 17.4, which indicates that it is not a factor causing failure. This is reinforced by the crystal orientation of (110), (211), which has a low probability (compressive) with values of 1.043 and 1.021. A high probability is obtained at the crystal orientation (200) with a value of 1.063 and indicates the presence of texture irregularities. Irregularity of texture can be suspected as a defect in the leaf spring. Defects can also be seen in the observation of fracture morphology by the appearance of voids. The voids are scattered randomly on the surface of the leaf spring and become the center of stress concentration. High-stress concentrations trigger crack nucleation. In addition, failure is also caused by fatigue, which can be observed in the morphology of the SEM fracture in the presence of striations. Hardness testing shows that the leaf spring material complies with the standardization of spring steel grade SUP 10 (406 – 448 HV).

References

Abdul, A., Yang, M., Shimizu, T., Furushima, T., 2021. Effect of Grain Misorientation and Martensitic Transformation on Surface Roughening Behavior in Thin Austenitic Stainless Steel Foils. *International Journal of Technology*, Volume 12(6), pp. 1161–1167

Ahn, Y.-K., Jeong, Y.-K., Kim, T.-Y., Cho, J.-U., Hwang, N.-M., 2020. Texture evolution of non-oriented electrical steel analyzed by EBSD and in-situ XRD during the phase transformation from γ to α. *Materials Today Communications*, Volume 25, p. 101307

Aliakbari, K., 2019. Failure Analysis of Base Plate Bolts of Radial Forging Machine. *Journal of Stress Analysis*, Volume 4(1), pp. 89–98

Andoko, A., 2019. The Effects of Strain Amplitude and Low Cycle Fatigue (LCF) Behavior on Nodular Cast Iron with Two-step Austempering (TSA) Process. *Materials Research Express*, 6(9), 095705

Andoko, A., Puspitasari, P., Permanasari, A.A., 2017. Analysis of Strength of Glass Fibre Composite Leaf Spring Using Finite Element Method. *Journal of Mechanical Engineering Science and Technology (JMEST)*, Volume (1), pp. 1–8

Anwar, M.S., Melinia, R.K., Pradisti, M.G., Siradj, E.S., 2021. Effect of Prior Austenite Grain-Size on the Annealing Twin Density and Hardness in the Austenitic Stainless Steel. *International Journal of Technology*, Volume 12(6), pp. 1149–1160

Bag, A., Lévesque, M., Brochu, M., 2020. Effect of Shot Peening on Short Crack Propagation in 300M Steel. *International Journal of Fatigue*, Volume 131, p. 105346

Božić, Ž., Schmauder, S., Wolf, H., 2018. The Effect of Residual Stresses on Fatigue Crack Propagation in Welded Stiffened Panels. *Engineering Failure Analysis*, Volume 84, pp. 346–357

Bruno, G., Efremov, A.M., Levandovskyi, A.N., Clausen, B., 2011. Connecting the Macro- and Microstrain Responses in Technical Porous Ceramics: Modeling and Experimental Validations. *Journal of Materials Science,* Volume 46, pp. 161–173

Bunge, H.-J., 2013. Texture Analysis in Materials Science: Mathematical Methods. In: *Butterworth-Heinemann 2rd Edition*

Chadwick, D.J., 2016. *Mechanism of Shot Peening Enhancement for The Fatigue Performance of AA7050-T7451.* Theses and Dissertations, Purdue University

Chen, Huang, C.-Y., Wang, Y.-T., Huang, C.-Y., Yen, H.-W., 2020. Role of the Crystallographic Texture in Anisotropic Mechanical Properties of a Newly-developed Hot-rolled Transformation-induced Plasticity (TRIP) Steel. *Materials Science and Engineering: A*, Volume 790, p. 139683

De-la-Rosa, C.E.F.,Trejo, M.H., Román, M.C., López, E.A., 2016. Effect of Decarburization on the Residual Stresses Produced by Shot Peening in Automotive Leaf Springs. *Journal of Materials Engineering and Performance*, Volume 25(7), p. 2596–2603

Fairfax, E.J., Steinzig, M., 2016. A Summary of Failures Caused by Residual Stresses. *In:* Residual Stress, Thermomechanics & Infrared Imaging, Hybrid Techniques and Inverse Problems, Volume 9, pp. 209–214. Springer International Publishing

Fragoudakis, R., Saigal, A., Savaidis, G., Malikoutsakis, M., Bazios, I., Savaidis, A., Pappas, G., Karditsas, S., 2013. Fatigue Assessment and Failure Analysis of Shot-peened Leaf Springs. *Fatigue Assessment And Failure Analysis. Fatigue & Fracture of Engineering Materials & Structures*, Volume 36(2), pp. 92–101

Fragoudakis, R., Savaidis, G., Michailidis, N., 2017. Optimizing the Development and Manufacturing of 56SiCr7 Leaf Springs. *International Journal of Fatigue*, Volume 103, pp. 168–175

Fuentes, J.J., Aguilar, H.J., Rodríguez, J.A., Herrera, E.J., 2009. Premature Fracture in Automobile Leaf Springs. *Engineering Failure Analysis*, Volume 16(2),pp. 648–655

Heidary, O., Mirzaee, O., Honarbakhsh Raouf, A., Borhani, E., 2020. Textu (AISI) 4130 Steel. *Materials Science and Engineering: A*, Volume 793, p. 139751

Hossain, R., Pahlevani, F., Quadir, M.Z., Sahajwalla, V., 2016. Stability of Retained Austenite in High Carbon Steel Under Compressive Stress: An Investigation from Macro to Nano Scale. *Scientific Reports*, Volume 6(1), p. 34958

Kadkhodapour, J., Butz, A., Rad, S.Z., 2011. Mechanisms of Void Formation During Tensile Testing in a Commercial, Dual-phase Steel. *Acta Materialia*, Volume 59(7), pp. 2575–2588

Kong, Y.S., Abdullah, S., Omar, M.Z., Haris, S.M., 2016. Failure Assessment of a Leaf Spring Eye Design Under Various Load Cases. *Engineering Failure Analysis*, Volume 63, pp. 146–159

Kurniawan, P., Andoko, A., Sunu, P.W., 2021. Leaf spring type simulation with finite element method approach. *Institute of Physics (IOP) Conference Series: Materials Science and Engineering*, Volume 1034(1), p. 012015

Li, X., Zhang, L., Dong, Y., Wei, Z., Que, Z., Qu, X., 2021. Orientation Relationship of Texture Development in Hot-rolled W During Annealing. *International Journal of Refractory Metals and Hard Materials*, Volume 97, p. 105527

Liu, Y., Yang, C.D., Liu, M., Wang, C.H., Dai, Y.C., Li, X., Russell, A.M., Zhang, C.X., Zhang, Z.H., Cao, G.H., 2018. Effects of Microstructure and Crystallography on Mechanical Properties of Cold-rolled SAE1078 Pearlitic Steel. *Materials Science and Engineering: A*, Volume 709, pp. 115–124

Manawan, M., Aritonang, S., Elita Hafizah, M.A., Hali, A.S., Darsono, N., Sudiro, T., Putro, P.A., Risdiana, R., 2021. XRD Residual Stress and Texture Analysis on 6082T Aluminum Alloy. *Materials Science Forum*, Volume 1028, pp. 409–414

Minamizawa, K., Arakawa, J., Akebono, H., Nambu, K., Nakamura, Y., Hayakawa, M., Kikuchi, S., 2022. Fatigue Limit Estimation for Carburized Steels with Surface Compressive Residual Stress Considering Residual Stress Relaxation. *International Journal of Fatigue*, Volume 160, p. 106846

Pástor, M., Lengvarský, P., Trebuňa, F., Čarák, P., 2020. Prediction of Failures in Steam Boiler using Quantification of Residual Stresses. *Engineering Failure Analysis*, Volume 118, p. 104808

Peng, W., Zhang, J., Yang, X., Zhu, Z., Liu, S., 2010. Failure Analysis on the Collapse of Leaf Spring Steels During Cold-punching. *Engineering Failure Analysis*, Volume 17(4), pp. 971–978

Priyanto, T.H., Effendi, N., Parikin., 2015. Texture Analysis of the Hot Rolling Austenitic Cr-Ni Steel Using Neutron Diffraction Method. *Advanced Materials Research*, Volume 1123, pp. 104–108

Purnama, D., Winarto, W., Sofyan, N., Prihastomo, A., Ito, K., 2020. Microstructure and Mechanical Properties of Ah-36 Steel Weldment Welded using Magnesium Modified E6013 Electrode. *International Journal of Technology*, Volume 11(1), pp. 48–59

Ren, P., Chen, X.P., Wang, C.Y., Zhou, Y.X., Cao, W.Q., Liu, Q., 2021. Evolution of Microstructure, Texture and Mechanical Properties of Fe–30Mn–11Al–1.2C Low-density Steel During Cold Rolling. *Materials Characterization*, Volume 174, p. 111013

Scuracchio, B.G., de-Lima, N.B., Schön, C.G., 2013. Role of Residual Stresses Induced by Double Peening on Fatigue Durability of Automotive Leaf Springs. *Materials and Design*, Volume 47, pp. 672–676

Shojaei, M., Khayati, G.R., Khorasani, S.M.J., Hernashki, R.K., 2021. Investigation of Spring Back Phenomenon in the 316L Stainless Steel Cathode Blank Based on the Changes in Electrical Resistivity and Magnetic Properties Due to the Residual Stress and Martensite Phase Formation: An Industrial Failure. *Engineering Failure Analysis*, Volume 126, p. 105473

Soyama, H., Chighizola, C.R., Hill, M.R., 2021. Effect of Compressive Residual Stress Introduced by Cavitation Peening and Shot Peening on the Improvement of Fatigue

Strength of Stainless Steel. *Journal of Materials Processing Technology*, Volume 288, p. 116877

Soyama, H., Kikuchi, T., Nishikawa, M., Takakuwa, O., 2011. Introduction of Compressive Residual Stress Into Stainless Steel by Employing a Cavitating Jet in Air. *Surface and Coatings Technology*, Volume 205(10), pp. 3167–3174

Wenk, H.R., 2016. Preferred Orientation in Deformed Metal and Rocks: An introduction to Modern Texture Analysis. In: *Academic Press,* Orlando, Florida

Xiao, G., Chen, B., Li, S., Zhuo, X., 2022. Fatigue Life Analysis of Aero-engine Blades for Abrasive Belt Grinding Considering Residual Stress. *Engineering Failure Analysis*, Volume 131, p. 105846

Xie, C., Liu, Z., He, X., Wang, X., Qiao, S., 2020. Effect of Martensite–austenite Constituents on Impact Toughness of Pre-tempered MnNiMo Bainitic Steel. *Materials Characterization,* Volume 161, p. 110139

Zhang, J., Di, H., Deng, Y., Misra, R.D.K., 2015. Effect of Martensite Morphology and Volume Fraction on Strain Hardening and Fracture Behavior of Martensite–ferrite Dual Phase Steel. *Materials Science and Engineering: A*, Volume 627, pp. 230–240

Zhang, Z., Hu, Z., Schmauder, S., Zhang, B., Wang, Z., 2019. Low Cycle Fatigue Properties and Microstructure of P92 Ferritic-martensitic Steel at Room Temperature and 873 K. *Materials Characterization*, Volume 157, p. 109923